Catalysis Today 141 (2009) 187–194

Contents lists available at ScienceDirect

Catalysis Today

journal homepage: www.elsevier.com/locate/cattod

The effect of zirconia polymorphs on the structure and catalytic properties of V_2O_5/ZrO_2 catalysts

Komandur V.R. Chary *, Kanaparthi Ramesh, Dhachapally Naresh, Pendyala Venkat Ramana Rao, A. Ramachandra Rao, Vattikonda Venkat Rao

Catalysis Division, Indian Institute of Chemical Technology, Tarnaka, Hyderabad 500607, India

ARTICLE INFO

Article history:
Available online 17 June 2008

Keywords:
Vanadia
Monoclinic zirconia
Tetragonal zirconia
Alkylation
Phenol

ABSTRACT

The effect of zirconia polymorphs on the activity and selectivity of V_2O_5/ZrO_2 for the alkylation of phenol with methanol has been investigated. Relatively pure monoclinic zirconia (m-ZrO_2) and tetragonal zirconia (t-ZrO_2) were prepared. A series of vanadium oxide supported on m- and t-ZrO_2 with varying vanadium oxide content from 2.5 to 15 wt% were prepared by wet impregnation method. The catalysts were characterized by X-ray diffraction (XRD), UV–vis diffuse reflectance spectroscopy (UV-DRS), temperature-programmed reduction of H_2 (TPR), temperature-programmed desorption (TPD) of NH_3, specific surface area and pore size distribution measurements. The XRD results suggest that highly dispersed or amorphous state of vanadium oxide is present at lower loadings. X-ray diffraction patterns also indicate the presence of crystalline V_2O_5 phase from 7.5 wt% of V_2O_5 on m-ZrO_2 support and there is no indication for the formation of V_2O_5 crystalline phase up to 15 wt% of V_2O_5 on t-ZrO_2 support. The UV–vis diffuse reflectance spectra indicate the existence of isolated and clusterized tetrahedral (Td) V^{5+} species at lower loadings in all catalysts. The temperature-programmed reduction of H_2 shows a single reduction peak corresponding to V^{5+} to V^{3+} in all the samples. TPD of ammonia suggests that surface acid density of m-ZrO_2 phase is found to be more than t-ZrO_2 phase. Acidity of the supported catalysts is increased with increase in V_2O_5 loading up to monolayer formation and decreased with the appearance of crystalline phase of V_2O_5. At monolayer coverage, V_2O_5/m-ZrO_2 is fourfold more active than V_2O_5/t-ZrO_2 for alkylation of phenol at 673 K. Selectively C-alkylated products were formed on all the catalysts. A linear correlation is observed between catalytic activity and surface acidity of catalysts.

1. Introduction

Alkylated phenols are important chemical intermediates in agrochemicals, pharmaceuticals, specialty plastics, and polymers. For example, *o*-cresol has applications in the synthesis of herbicides, 2,6-xylenol in the manufacture of polyphenylene oxide (PPO) and special-grade paints [1,2] and 2,3,6-trimethyl phenol in the synthesis of vitamin-A, etc. Alkylation of phenol with methanol over oxides and zeolites indicates that the reaction is sensitive to acidic and basic properties of catalysts [3–7] that would effect the product selectivity. A few investigations were reported on supported vanadia catalysts for alkylation of phenolic compounds [8–11]. The catalytic properties of the active vanadium oxide phase can be greatly influenced by the nature of the supported oxide and its dispersion on the support material. ZrO_2 is an excellent support for the synthesis of highly dispersed oxides when compared to weakly interacting supports such as SiO_2. ZrO_2 also inhibits sintering of supported oxides in the presence of water and high temperature [12]. Moreover ZrO_2 consist special characteristics such as high thermal stability, extreme hardness, acidic/basic features and stability under reducing conditions. It is well known that ZrO_2 exists mainly in three polymorphs with monoclinic (m-ZrO_2), tetragonal (t-ZrO_2) and cubic structures. High isomerization activity and low dehydrogenation activity of *n*-butane was reported over Pt/ZrO_2-WO_x containing a large fraction of t-ZrO_2 [13]. Jung and Bell [14] emphasized that ZrO_2 phase could influence the activity of Cu/ZrO_2 catalysts in methanol synthesis. Pokrovoski et al. [15] also reported from IR and TPD studies that adsorption process of CO and CO_2 on m-ZrO_2 and t-ZrO_2 were different in several respects. These considerable differences in catalytic functionalities between m- and t-ZrO_2 prompted us to investigate the nature of polymorphs of zirconia as support materials in supported vanadia catalysts during alkylation reactions.

In the present investigation, we report a systematic study on the characterization of vanadia catalysts supported on monoclinic and tetragonal zirconia by X-ray diffraction (XRD), BET surface area, pore

* Corresponding author. Tel.: +91 40 27193162; fax: +91 40 27160921.
E-mail address: kvrchary@iict.res.in (Komandur V.R. Chary).

0920-5861/$ – see front matter © 2008 Elsevier B.V. All rights reserved.
doi:10.1016/j.cattod.2008.04.014

size distribution (PSD), UV–vis diffuse reflectance spectroscopy (UV-DRS), temperature-programmed reduction (TPR) and temperature-programmed desorption (TPD) of NH_3. The catalytic properties were evaluated for vapour phase alkylation of phenol with methanol.

2. Experimental

2.1. Catalyst preparation

A series of V_2O_5/ZrO_2 (monoclinic and tetragonal) catalysts with V_2O_5 loading in the range of 2.5–15 wt% were prepared by wet impregnation method with requisite amounts of ammonium metavanadate dissolved in oxalic acid solution. The m-ZrO_2 support (BET surface area 44 m^2/g) prepared from zirconium hydroxide was obtained from MEL chemicals (681/01) and calcined at 773 K for 5 h before use. The single-phase t-ZrO_2 was prepared by the addition of 5 M NaOH drop wise to zirconyl nitrate (0.4 M) at 353 K and pH 14. A white precipitate thus formed was kept for aging for 17 h. The resultant cake was washed with double distilled water till the pH reaches to 7. It was oven dried for 16 h and calcined at 773 K for 5 h to obtain relatively pure t-ZrO_2.

2.2. Catalyst characterization

X-ray diffraction (XRD) studies were carried out on a Philips PW 1051 diffractometer using Ni-filtered Cu Kα radiation. Identification of the phases was made with the help of the Joint Committee on Powder Diffraction Standard (JCPDS) files.

Specific surface areas were measured by static method using an all pyrex glass system capable of attaining 10^{-6} Torr pressure. The specific surface areas of the catalysts were determined by the BET method using nitrogen physisorption at 77 K taking 0.162 nm^2 as its cross-sectional area. Pore size distribution measurements were performed on an Auto pore III (Micromeritics) by mercury penetration method.

UV–vis spectra were recorded in air at room temperature using a GBC UV-Visible Cintra 10_e spectrometer with a diffuse reflectance accessory, in 200–800 nm wavelength range. The Kubelka-Munk function $F(R)$ was plotted against the wavelength. Temperature-programmed reduction of H_2 and also temperature-programmed desorption of NH_3 were carried out as per the procedure described elsewhere [16,17].

2.3. Catalytic activity

The catalytic performance of vanadia catalysts supported on m- and t-ZrO_2 has been tested for the vapour phase alkylation of phenol. Activity runs were carried out in a vertical fixed bed, continuous down flow reactor at 673 K under atmospheric pressure as described in our earlier paper [8]. In a typical experiment, ca. 0.5 g of catalyst was packed between the layers of quartz wool, and the upper portion of the reactor was filled with glass beads, which served as pre-heaters for the reactants. The catalyst was kept under activation at 673 K in N_2 flow (40 mL/min) for 2 h. The products were mainly 2,6-xylenol and *o*-cresol together with trace amounts of higher alkylated products.

3. Results and discussion

3.1. X-ray diffraction

X-ray diffraction patterns of various V_2O_5/m-ZrO_2 catalysts with vanadia loadings ranging from 2.5 to 12.5 wt% are shown in Fig. 1. It can be seen in Fig. 1 that all the samples showed XRD peaks due to monoclinic zirconia with major peaks at d = 3.16 and 2.834 Å (JCPDS No. 37-1484). For samples <7.5 wt% V_2O_5, no XRD peaks corresponding to vanadium oxide crystallites were observed. It indicates that vanadium oxide is present in a highly dispersed or amorphous state within 7.5 wt% V_2O_5 loading on m-ZrO_2. However, XRD peaks corresponding to V_2O_5 at 2θ = 20.26 can be seen from 7.5 wt% sample, and its intensity is found to increase with increase of vanadia loading. The amount of vanadia needed for total coverage of support (as 2D monolayer) was estimated to be 0.145 wt% of V_2O_5 per m^2 of the support surface [18]. Therefore, m-ZrO_2 support having surface area 44 m^2/g requires a quantity of 6.38 wt% V_2O_5 to yield a single monolayer. In the present study, V_2O_5 crystallites started appearing from 7.5 wt% of V_2O_5. These results are in good agreement with the theoretical monolayer calculations. From 12.5 wt% of vanadia loading, XRD peaks corresponding to ZrV_2O_7 were observed at lower d values, which is due to strong interaction between active vanadia and monoclinic zirconia support. Male et al. [19] and Su and Bell [20] also reported the formation of such ZrV_2O_7 spinals at higher loadings of vanadium oxide supported on zirconia.

The X-ray diffraction patterns of various V_2O_5/t-ZrO_2 catalysts with vanadia loadings ranging from 2.5 to 15 wt% are shown in Fig. 2. As can be seen from Fig. 2 the characteristic peak at d = 2.993 and 1.80 Å suggests the presence of only tetragonal phase in all the samples (JCPDS No. 27-997). There are no characteristic peaks corresponding to vanadium oxide in these samples indicating that vanadium oxide is present in highly dispersed amorphous state. According to the theoretical monolayer calculations [18], t-ZrO_2 support having surface area 117 m^2/g requires a quantity of 16.96 wt% V_2O_5 to yield a single monolayer. Our results are well in agreement with the theoretical monolayer calculations. The present XRD results also indicate that there is no compound formation between t-ZrO_2 and V_2O_5.

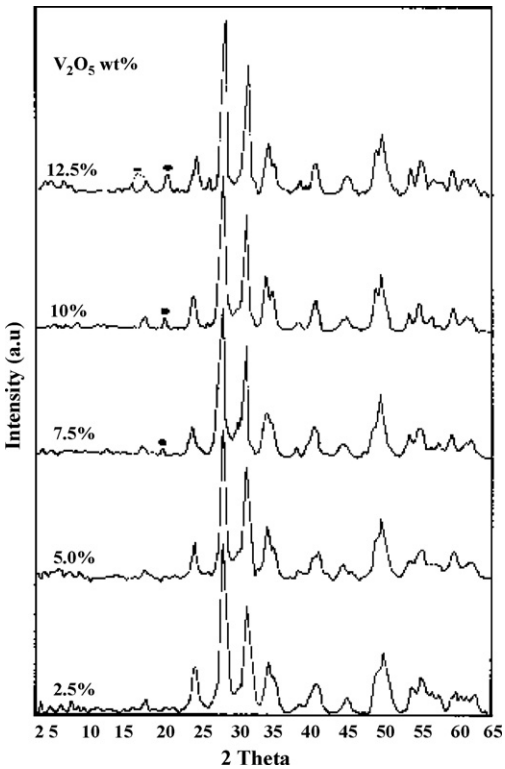

Fig. 1. X-ray diffraction patterns of various V_2O_5/m-ZrO_2 catalysts. (●) V_2O_5 diffraction lines; (■) ZrV_2O_7 diffraction lines.

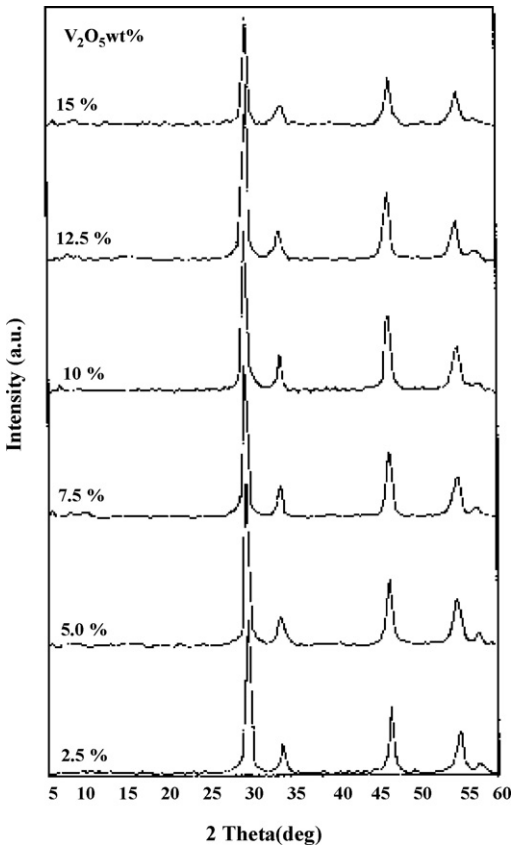

Fig. 2. X-ray diffraction patterns of various V_2O_5/t-ZrO_2 catalysts.

3.2. BET surface area and pore size distribution

The surface areas of the pure m-ZrO_2 and pure t-ZrO_2 are found to be 44 and 117 m^2/g, respectively. Tables 1 and 2 show the effect of V_2O_5 content on the values of the specific surface area (S_{BET}) of V_2O_5/m-ZrO_2 and V_2O_5/t-ZrO_2 catalysts, respectively. The S_{BET} of V_2O_5/m-ZrO_2 and V_2O_5/t-ZrO_2 catalysts are increased for 2.5 and 5 wt% catalysts when compared to pure supports. The further increases of the V_2O_5 loading S_{BET} values are decreased. At low V_2O_5 content (2.5 and 5 wt%), in principle, two phenomena could be acting. One is the interconnection between original ZrO_2 grains by the impregnated V_2O_5 and the other is the simultaneous filling of ZrO_2 pores. These two effects cooperate each other to aggregating the resultant particles. Subsequently they produce small aggregates during calcinations leading to increase in the surface area as observed. At higher V_2O_5 loadings, the partial blockage of pores of zirconia by

Table 1
The results of BET surface area and pore size distribution measurements of various V_2O_5/m-ZrO_2 catalysts

V_2O_5 loading (wt%)	BET surface area (m^2/g)	Pore volume (mL/g)	Total pore area (m^2/g)	V surface density (m^2)
0.0	44	0.54	63	0
2.5	52	0.50	72	159.0
5.0	49	–	–	337.5
7.5	44	0.36	55	563.8
10.0	40	–	–	826.9
12.5	36	0.39	48	1148.5

V surface density = V_2O_5 percentage $\times$ $6.02 \times 10^{23}/S_{BET} \times 182 \times 10^{18}$.

Table 2
The results of BET surface area and pore size distribution measurements of various V_2O_5/t-ZrO_2 catalysts

V_2O_5 loading (wt%)	BET surface area (m^2/g)	Pore volume (mL/g)	Total pore area (m^2/g)	V surface density (m^2)
0.0	117	0.402	113	0
2.5	124	0.313	115	0.66
5.0	121	0.336	124	136.7
7.5	114	0.236	92	217.6
10.0	106	0.209	84	312.0
12.5	97	0.205	95	426.2
15.0	92	0.201	83	539.3

V surface density = V_2O_5 percentage $\times$ $6.02 \times 10^{23}/S_{BET} \times 182 \times 10^{18}$.

crystalline V_2O_5 phase or V–Zr interactions could be responsible for the gradual decrease of the surface areas in all the catalysts [21,22]. The formation of the crystalline V_2O_5 and ZrV_2O_7 (V_2O_5/m-ZrO_2 catalysts) at higher V/Zr ratio was conformed by XRD. The total pore area and pore volume of samples measured by mercury penetrating porosimeter has been presented in Tables 1 and 2, respectively. The total pore area decreased with increase in vanadia loading in the similar lines of surface areas of the catalysts.

The V surface density [V surface density = V_2O_5 percentage $\times$ $6.02 \times 10^{23}/S_{BET} \times 182 \times 10^{18}$] was calculated using method reported by Chen et al. [21] for MoO_3/ZrO_2 catalysts. Tables 1 and 2 show the effect of V_2O_5 loadings on the apparent V surface density. With increase of V_2O_5 loading V surface density is increased due to concomitant decrease in the surface area of zirconia. Surface density calculations are well correlated with the theoretical monolayer calculations. In the V_2O_5/m-ZrO_2 catalysts, the surface density is found to be 564 m^2 for 7.5 wt% V_2O_5 catalyst wherein the XRD peaks corresponding to V_2O_5 crystallites appeared. However, the surface density is 539 m^2 for 15 wt% V_2O_5 catalyst in the V_2O_5/t-ZrO_2 catalysts which is lower than 7.5 wt% V_2O_5/m-ZrO_2 catalyst. Due to this reason, crystalline V_2O_5 peaks might have observed at 7.5 wt% V_2O_5 loading in V_2O_5/m-ZrO_2 catalysts.

3.3. UV–vis diffuse reflectance spectroscopy

The DR-UV–vis spectra of V_2O_5/m-ZrO_2 and V_2O_5/t-ZrO_2 catalysts are shown in Figs. 3 and 4. The charge transfer (CT) spectra of V^{5+} ions (d^0) were recorded between 200 and 800 nm for m-ZrO_2 and t-ZrO_2 supported VO_x catalysts containing 2.5–15 wt% of V_2O_5. In all the catalysts the spectrum is dominated by two charge transfer (CT) bands of V^{5+} (d^0) at 290 and 370 nm with good resolution. The energy of oxygen → vanadium charge transfer (LMCT, Zr–O → V^{5+}) absorption band, which is correlated with the minimum diffuse reflectance, is strongly influenced by the number of ligands surrounding the central vanadium ion. Thus, it can be used to obtain very useful information on the coordination of vanadium ions in different surface species [23,24]. The spectral features of the catalysts, consisting of an absorption band at 290 nm arise from the charge transfer in di-or oligomeric structures formed by the condensation of monomeric species and V^{5+} ion in tetrahedral coordination [23]. The charge transfer band at ~370 nm in all the systems is due to V^{5+} ions coordinated by five oxygen ligands in the form of a square pyramidal [23] and with increasing vanadium loading, the band (~370) is shifted to higher wavelength region. Thus, the present results suggest that the dispersed vanadia consists of isolated tetrahedral units at lower vanadium loadings and the crystalline vanadia is in the form of distorted octahedral vanadia at higher loadings.

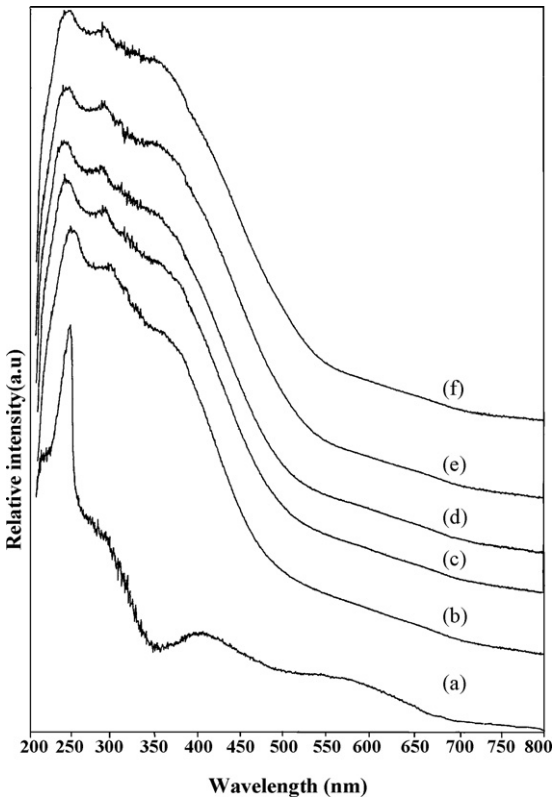

Fig. 3. UV–vis diffuse reflectance spectra of various V_2O_5/m-ZrO_2 catalysts: (a) 0.0% V_2O_5; (b) 2.5% V_2O_5; (c) 5.0% V_2O_5; (d) 7.5% V_2O_5; (e) 10.0% V_2O_5; (f) 12.5% V_2O_5.

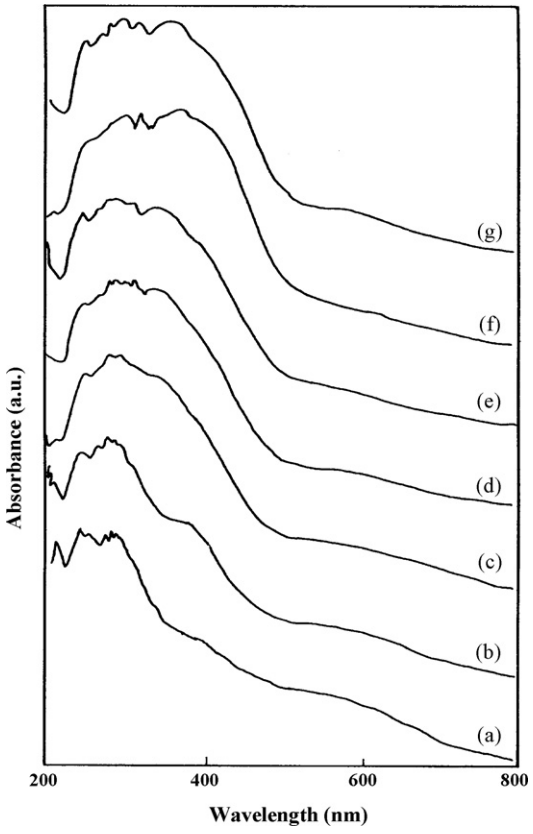

Fig. 4. UV–vis diffuse reflectance spectra of various V_2O_5/t-ZrO_2 catalysts: (a) 0.0% V_2O_5; (b) 2.5% V_2O_5; (c) 5.0% V_2O_5; (d) 7.5% V_2O_5; (e) 10.0% V_2O_5; (f) 12.5% V_2O_5; (g) 15.0% V_2O_5.

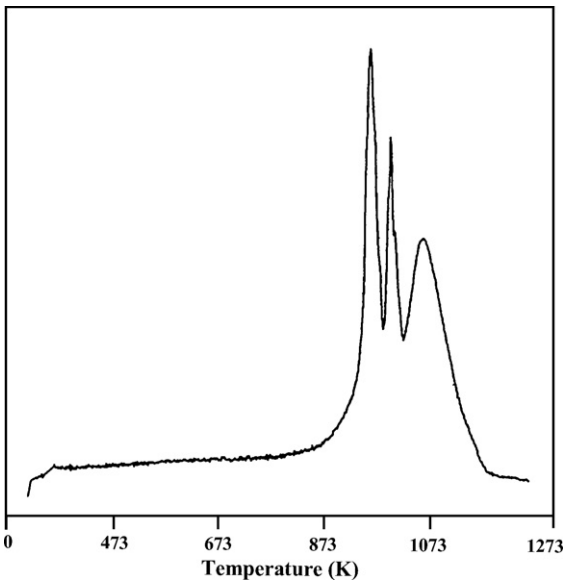

Fig. 5. Temperature-programmed reduction profiles of pure V_2O_5.

3.4. Temperature programmed reduction

TPR profile of unsupported V_2O_5 is shown in Fig. 5. According to the literature [25,26] the bulk vanadium oxide reduces at much higher temperature when compared to supported catalysts. They have attributed this phenomenon to the following reduction sequence. The sharp peak at 965 K corresponds to the reduction of V_2O_5 to

$$V_2O_4 \rightarrow V_2O_3 \rightarrow V_2O_5 \rightarrow V_6O_{13}$$

V_6O_{13} (first peak), the peak at 1003 K is associated with the reduction of V_6O_{13} to V_2O_4 (second peak), and the third peak at 1067 K corresponds to V_2O_3 formed by the reduction of V_2O_4.

H_2-TPR profiles of V_2O_5/m-ZrO_2 and V_2O_5/t-ZrO_2 samples are shown in Figs. 6 and 7. The results of TPR by various V_2O_5/m-ZrO_2 and V_2O_5/t-ZrO_2 catalysts show a schematic change in the reduction of vanadia with increase of vanadia loading. The TPR profiles for all samples have shown only one prominent peak (T_{max}) corresponding to V^{5+} to V^{3+}. TPR of unsupported V_2O_5 (Fig. 5) reveals that it reduces at higher temperature when compared to V_2O_5/m-ZrO_2 and V_2O_5/t-ZrO_2 catalysts which is in consistent with the work of Koranne et al. [25] and Bosch et al. [26]. These authors reported that supported vanadium oxide catalysts reduce at much lower temperature than bulk vanadia and the reducibility of vanadia is strongly influenced by the kind of support used. Baiker et al. [27] also reported that titania supported vanadium oxide catalysts exhibited only one reduction peak during TPR, if less than four layers of vanadium oxide was deposited. Our previous studies [28] confirm such observation. Bond et al. [29] also reported that the VO_x monolayer species are reduced in a single step from V^{5+} to V^{3+}. From Figs. 6 and 7 and Tables 3 and 4, it has been observed that the T_{max} values are increased from 700 to 738 K and 668 to 786 K with increase of vanadia loading in the case of V_2O_5/m-ZrO_2 and V_2O_5/t-ZrO_2 catalysts, respectively. The shift in reduction temperature indicates that the reducibility of vanadia decreases with loading on m-ZrO_2 and t-ZrO_2. The amount of hydrogen consumption in V_2O_5/t-ZrO_2 is much higher than V_2O_5/m-ZrO_2 catalysts. The high hydrogen consumption may be due to partial reduction of t-ZrO_2 in the TPR procedure sequences with the V_2O_5. A second reduction peak at 1100 K with V_2O_5/t-ZrO_2 catalysts was observed. This peak may be due to the reduction of pure t-ZrO_2

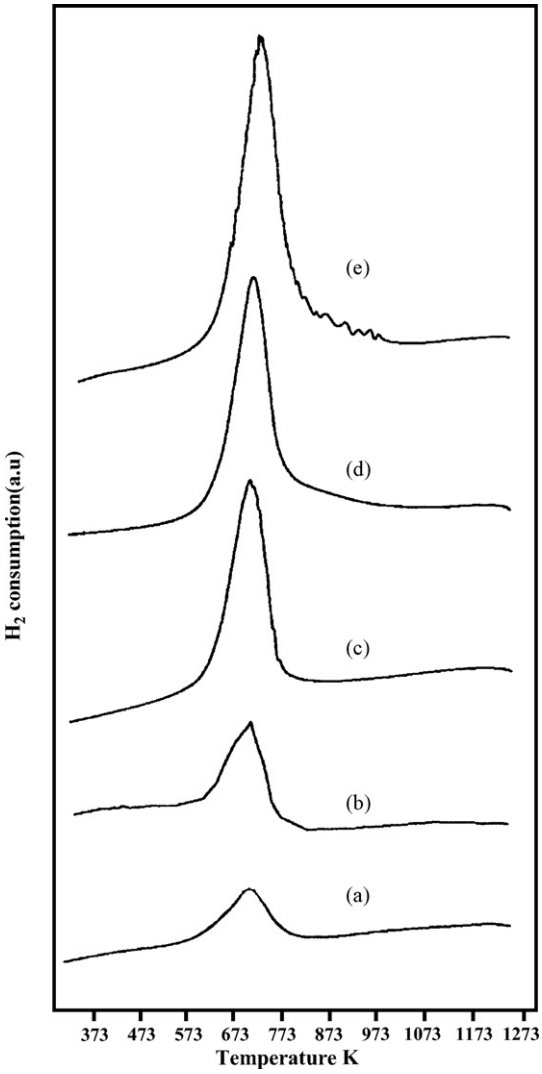

Fig. 6. Temperature-programmed reduction profiles of various V_2O_5/m-ZrO_2 catalysts: (a) 2.5% V_2O_5; (b) 5.0% V_2O_5; (c) 7.5% V_2O_5; (d) 10.0% V_2O_5; (e) 12.5% V_2O_5.

Table 3
Temperature-programmed reduction (TPR) results of various V_2O_5/m-ZrO_2 catalysts

V_2O_5 loading (wt%)	T_{max} (K)	H_2 consumption (mL/g)
2.5	713	5.53
5.0	700	8.20
7.5	710	16.69
10.0	717	18.08
12.5	738	34.29

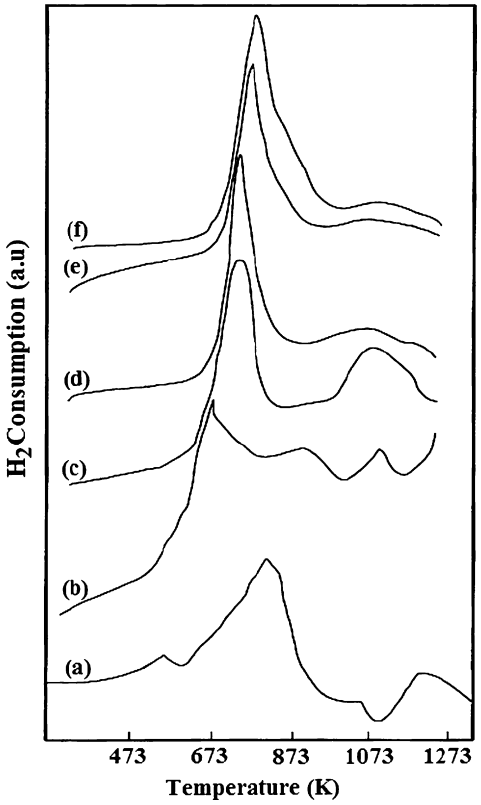

Fig. 7. Temperature-programmed reduction profiles of various V_2O_5/t-ZrO_2 catalysts: (a) 2.5% V_2O_5; (b) 5.0% V_2O_5; (c) 7.5% V_2O_5; (d) 10.0% V_2O_5; (e) 12.5% V_2O_5; (f) 15.0% V_2O_5.

support. The observed support reduction is further supported with high hydrogen consumption. Thus TPR results suggest that the interaction of vanadia with zirconium oxide is stronger at lower vanadia loadings. TPR results are also well correlated with the XRD and UV-DRS results.

Fig. 8 shows the variation of H_2 consumption and vanadia surface density. The results suggest the reducibility of V_2O_5 increases with increasing surface density in the sample irrespective of the support used. V_2O_5/t-ZrO_2 show higher V surface density compared to the V_2O_5/m-ZrO_2 catalysts.

3.5. Temperature programmed desorption of NH_3

Temperature-programmed desorption (TPD) of ammonia and/or pyridine is a popular method for the determining the acidity of solid catalysts as well as acid strength distribution. Ammonia is frequently used as a probe molecule because of its small molecular size, stability and strong basic strength (pK_a = 9.2). In the present investigation, the acidity measurements have been carried out by NH_3-TPD method. The acid amount and acid density of V_2O_5/m-ZrO_2 catalysts measured by temperature-programmed desorption

Table 4
Temperature-programmed reduction (TPR) results of various V_2O_5/t-ZrO_2 catalysts

V_2O_5 loading (wt%)	T^1_{max} (K)	H_2 consumption (mL/g)	T^2_{max} (K)	H_2 Consumption (mL/g)
2.5	824	42.4	–	–
5.0	668	50.7	1091	4.4
7.5	727	52.2	1102	21.0
10.0	747	106.0	1092	19.8
12.5	784	186.8	1140	14.6
15.0	786	189.5	1137	12.6

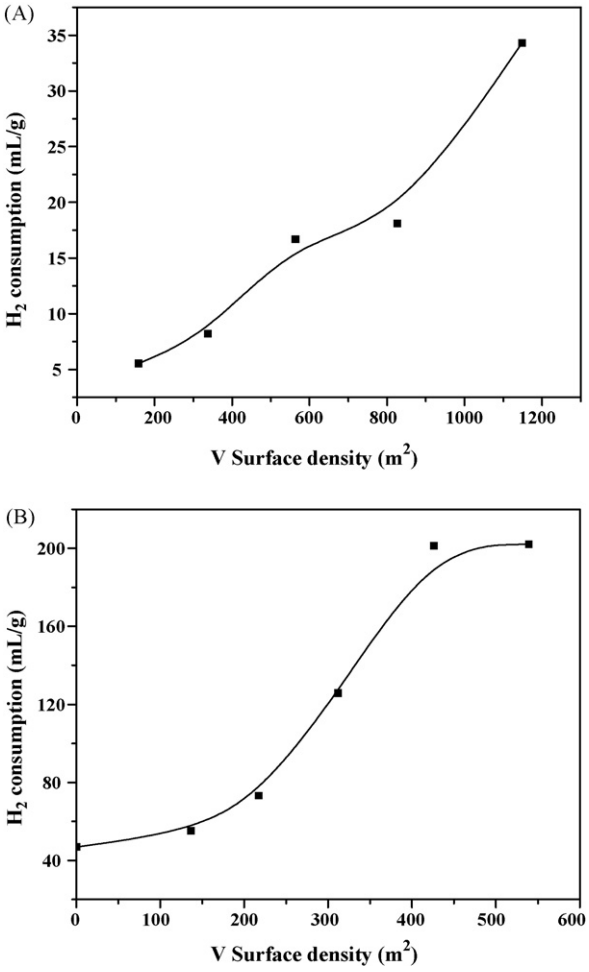

Fig. 8. A relation between H_2 consumption and V surface density over various V_2O_5/ZrO_2 catalysts: (A) m-ZrO_2 and (B) t-ZrO_2.

of NH_3 method are given in Table 5. From the peak positions, it is clear that desorption of NH_3 is associated in two temperature regions corresponding to weak and moderate acid strengths (Lewis and Bronsted acid sites). As it can be noted in Table 5 both the acidity and acid density of the catalysts were found to increase with V_2O_5 loading up to 7.5 wt% V_2O_5 due to highly dispersed state V_2O_5 and to decrease beyond 7.5 wt% V_2O_5 due to formation of crystalline phase. Moreover, ZrV_2O_7 spinel was also observed at high V_2O_5 loading (Fig. 1). Comparing the results of acidity measurements and XRD, it can be seen that, dispersed V_2O_5 below the monolayer coverage forms V–O–Zr surface species on m-ZrO_2. At higher V_2O_5 loading, it leads to sintering of zirconia surface due to transformation of V–O–Zr surface species into bulk ZrV_2O_7. Accordingly the formation of V–O–Zr surface species could be

Table 5
Temperature-programmed desorption (TPD) of NH_3 results of various V_2O_5/m-ZrO_2 catalysts

V_2O_5 loading (wt%)	T_{des} (K)	Total acidity (mL/g)	Acid density ($N_{acid\ sites}/m^2$) × 10^{17}
0.0	599	4.6	28.09
2.5	605	7.3	37.72
5.0	603	9.8	53.74
7.5	600	11.4	69.62
10.0	606	11.2	75.24
12.5	599	9.8	73.15

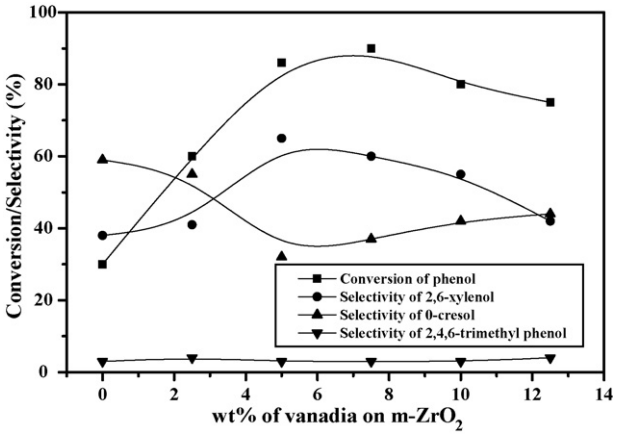

Fig. 9. Alkylation of phenol with methanol over various V_2O_5/m-ZrO_2 catalysts.

Table 6
Temperature-programmed desorption (TPD) of NH_3 results of various V_2O_5/t-ZrO_2 catalysts

V_2O_5 loading (wt%)	T_{des} (K)	Total acidity (mL/g)	Acid density ($N_{acid\ sites}/m^2$) × 10^{17}
0.0	550	3.13	7.18
2.5	548	3.58	7.75
5.0	552	3.87	8.59
7.5	556	4.07	9.59
10.0	560	4.34	11.0
12.5	559	4.61	12.77
15.0	560	4.14	12.09

responsible for the acidity of V_2O_5/m-ZrO_2 catalysts. Interestingly, these results are also reflected in the conversion of phenol and the selectivity towards 2,6-xylenol as shown in Fig. 9.

The acidity and acid density of V_2O_5/t-ZrO_2 catalysts measured by TPD of NH_3 are given in Table 6. From the peak positions, it is clear that desorption of NH_3 in these catalysts is associated to only one temperature region which corresponds to moderate acid strength. The acidity of the catalysts was found to increase with V_2O_5 loading up to 12.5 wt% of V_2O_5 and decreased with further increase in vanadia content. The decrease in acidity above 12.5 wt% may be due to on set of microcrystallites of vanadium. The conversion of phenol with methanol and the selectivity towards 2,6-xylenol were observed in the same trend as shown in Fig. 10.

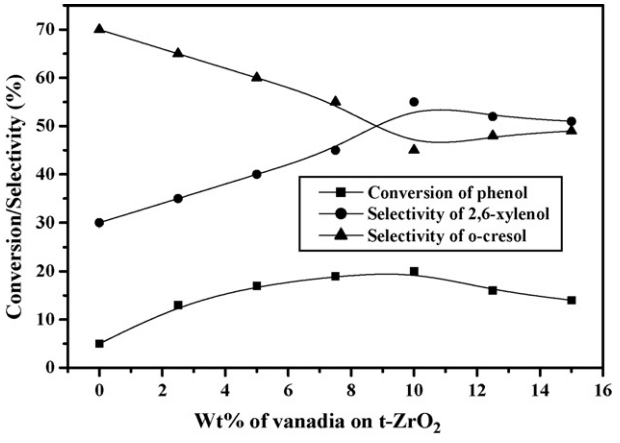

Fig. 10. Alkylation of phenol with methanol over various V_2O_5/t-ZrO_2 catalysts.

The acidity of vanadia supported on m-ZrO_2 catalysts is higher than supported t-ZrO_2 catalysts. The acid density of m-ZrO_2 supported catalysts is approximately four times more than t-ZrO_2 supported catalysts (28.09 and 7.18 μmol NH_3/m^2 on V_2O_5/m-ZrO_2 and t-ZrO_2, respectively). The higher acidity of V_2O_5/m-ZrO_2 is attributed to the presence of high concentration of anionic vacancies on the surface of m-ZrO_2. Such vacancies expose CUS-Zr^{4+} cations which act as Lewis acid centers and assist to enhance the Bronsted acidity of adjacent Zr-OH groups, which otherwise only weakly acidic. Thus the creation of accessibility to CUS-Zr^{4+} sites in combination with adjacent Bronsted acidic Zr–OH groups contribute to higher acidity and adsorption of NH_3 on m-ZrO_2 supported catalysts when compared to t-ZrO_2 supported catalysts. Zhao et al. [30] also reported comparison of surface acidic features between tetragonal and monoclinic nanostructured zirconia catalysts and concluded that the surface acidity is proportional to Zr^{4+} density. Thus, the acidity measurements are in good agreement with the phenol alkylation activity results.

3.6. Alkylation of phenol with methanol

Phenol alkylated products are governed by the type of phenol adsorption on the catalysts surface, depending on its acidic strength. On highly acidic or strong Brönsted acid sites, the phenol ring takes a position parallel to the surface as shown in Scheme 1. In this case, all the activated positions of phenol are available for the reaction resulting to substitution in the *ortho*, *meta*, as well as *para* positions in addition to the formation of ethers. Here, the selectivity mainly depends on the distance between acid sites and acidic strength. In the case of less acidity or Lewis acid sites coupled with basic sites, phenol ring adsorbs vertically and dissociatively to the surface giving preference to an attack in the *ortho* position or on oxygen of phenol as shown in Scheme 2. If the catalyst is more acidic the preferable attack of phenol is parallel, which causes more alkylated products or if the catalyst is less acidic the preferable attack of phenol is perpendicular, which causes less alkylated products. This is inconsistent with the observation of trimethyl phenol formation on V_2O_5/m-ZrO_2 catalysts, which are more acidic than V_2O_5/t-ZrO_2 catalysts.

Activity and selectivity during the vapour phase alkylation of phenol over V_2O_5/m-ZrO_2 catalysts are shown in Fig. 9. The conversion was found to increase with vanadia loading up to 7.5 wt% and decreased with further increase in vanadia loading. The increase of conversion with vanadia loading up to 7.5 wt% is attributed to increase of active vanadia sites due to monolayer formation. At higher loadings (above monolayer), vanadia crystallites are formed which reduce the activity. During the reaction only

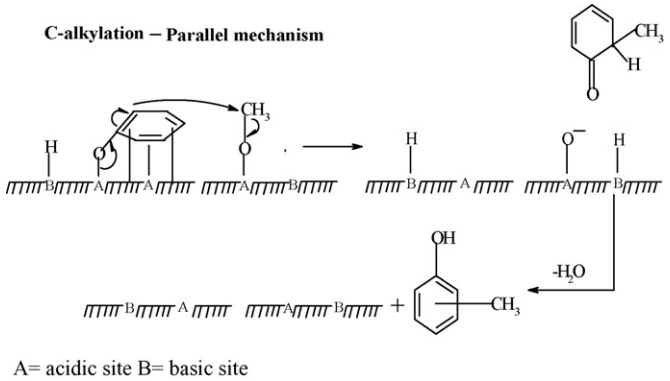

Scheme 1. Alkylation of phenol with methanol via parallel mechanism over vanadia supported catalysts.

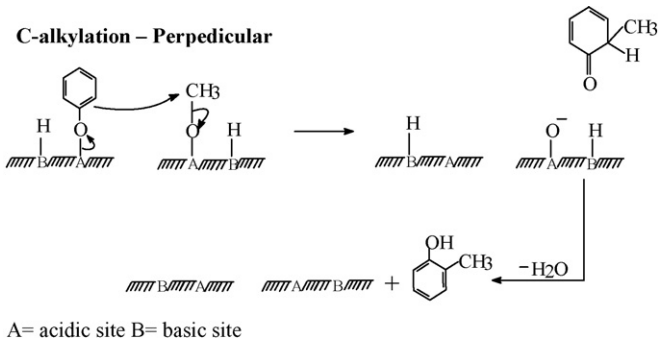

Scheme 2. Alkylation of phenol with methanol via perpendicular mechanism over vanadia supported catalysts.

C-alkylated products of phenol were formed. The selectivity of *o*-cresol decreases and the selectivity of 2,6-xylenol increases with vanadia content up to 7.5 wt%. Trimethyl phenol was also formed during the reaction and the selectivity towards this remained constant even at higher vanadia content. In the present investigation, we observed mainly *ortho*-products. This could be due to the reaction proceeding through an attack of methyl carbocation of methanol at *ortho* position of the ring rather than oxygen of phenol. Such reaction pathway for the methylation of phenol over hydrotalcites was also described in the literature [31]. Since the formation of 2,6-xylenol takes place via *o*-cresol, the increase in selectivity of former will be at the expense of the latter. The activity results suggest that pure m-ZrO_2 is also active for the reaction and the selectivity towards *o*-cresol is higher than supported vanadium oxide catalysts.

The activity of V_2O_5/t-ZrO_2 catalysts during alkylation of phenol with methanol is shown in Fig. 10. The activity of alkylation of phenol with methanol was increased with increase in vanadia loading up to 10 wt% and decreased with further increase in vanadia loading. The decrease in activity at higher loadings can be

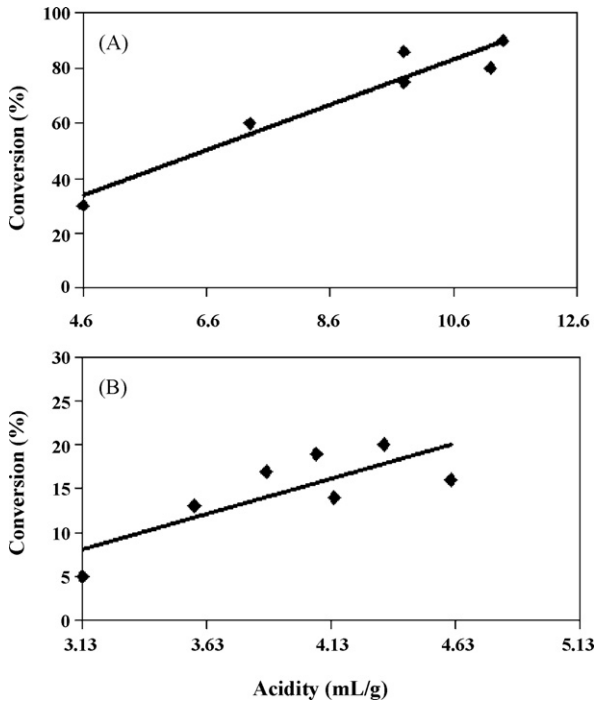

Fig. 11. A relation between acidity and alkylation activity over various V_2O_5/ZrO_2 catalysts: (A) m-ZrO_2 and (B) t-ZrO_2.

directly related to the decrease in acidity with vanadia loading. The increase in activity with the addition of vanadia is due the generation of moderate acid sites over the surface. These sites are due to Bronsted type of acid sites. The selectivity of *o*-cresol decreases with vanadia loading up to 10 wt% and remains constant beyond this loading. The selectivity of 2,6-xylenol increases with vanadia content up to 10 wt% of V_2O_5 and less significant at higher loadings. The constant selectivity at higher V_2O_5 loadings might be due to formation of vanadia crystallites on the surface, which decrease the acidity.

The activity of V_2O_5/m-ZrO_2 catalysts during alkylation of phenol with methanol was found to be approximately fourfold when compared to V_2O_5/t-ZrO_2 catalysts. The high activity of V_2O_5/m-ZrO_2 catalysts is due to more acidic nature of the catalysts. In the present study, conversion of phenol increased linearly with acidity up to a certain limit and at higher acidities, the conversion was independent of acidity. A relation between acidity and alkylation of phenol activity over vanadia supported on monoclinic and tetragonal zirconia catalysts are shown in Fig. 11. The alkylation of phenol activity is directly proportional to the acid density of the catalysts.

4. Conclusions

The ZrO_2 oxide is an interesting support to investigate the structural and acidic properties of zirconia polymorphs supported vanadium oxide catalysts. The XRD and UV-DRS results suggest that vanadium oxide is present in a highly dispersed or amorphous state on m-ZrO_2 support at lower vanadia loadings. The ZrV_2O_7 phase was observed at higher vanadium loading which clearly indicates that the strong metal–support interaction of V_2O_5/m-ZrO_2 catalysts. TPR results demonstrate that the reducibility of vanadia decreases with increase of vanadia loading. The total acidity of the catalysts increased up to monolayer formation and decreases further with increase of vanadium loading. The increase of acidity with V_2O_5 loading is due to formation of V–O–Zr species of the catalysts surface. The acidity of the m-ZrO_2 catalysts is higher than t-ZrO_2 supported catalysts due to spatial structural properties of m-ZrO_2. Vapour phase alkylation of phenol with methanol was investigated over V_2O_5 supported on m- and t-zirconia catalysts prepared by wet impregnation method. The highest catalytic activity was obtained on V_2O_5/m-ZrO_2 catalysts, which is due to high acidity of the catalysts. The alkylation activity increases up to 7.5 wt% over V_2O_5/m-ZrO_2 catalysts and 10 wt% on V_2O_5/t-ZrO_2 catalysts. The catalytic activity during vapour phase alkylation of phenol with methanol is directly related to the total acidity of the catalysts. The highest selectivity towards 2,6-xylenol is found on 7.5 wt% V_2O_5/m-ZrO_2 catalysts and 10 wt% V_2O_5/t-ZrO_2 catalysts.

Acknowledgements

The author D.N. thanks Council of Scientific and Industrial research (CSIR), New Delhi for the award of Senior Research Fellowship (SRF). PVRR thanks to the Director IICT for a project assistant position.

References

[1] sixth ed., Ullmann's Encyclopedia of Industrial Chemistry, vol. 9, Wiley–VCH, Weinheim, 2003, p. 642.
[2] K. Weissermel, H.J. Arpe, Industrial Organic Chemistry, Verlag Chemie, Weinheim, 1978, p. 316.
[3] S. Balsama, P. Beltrame, P.L. Beltrame, P. Carniti, L. Forni, G. Zuretti, Appl. Catal. A: Gen. 13 (1984) 161.
[4] P. Beltrame, P.L. Beltrame, P. Carniti, A. Castelli, L. Forni, Appl. Catal. A: Gen. 29 (1987) 327.
[5] B.M. Devassy, G.V. Shanbhag, S.B. Halligudi, J. Mol. Catal. A: Chem. 247 (2006) 162.
[6] B. Gopal Mishra, G. Ranga Rao, Micropor. Mesopor. Mater. 70 (2004) 43.
[7] K.M. Malshe, P.T. Patil, S.B. Umbarkar, M.K. Dongare, J. Mol. Catal. A: Chem. 212 (2004) 337.
[8] K.V.R. Chary, K. Ramesh, G. Vidyasagar, V. Venkat Rao, J. Mol. Catal. A: Chem. 198 (2003) 195.
[9] V. Venkat Rao, K.V.R. Chary, V. Durgakumari, S. Narayanan, Appl. Catal. A: Gen. 61 (1990) 89.
[10] S. Narayanan, V. Venkat Rao, V. Durgakumari, J. Mol. Catal. A: Chem. 52 (1989) L29.
[11] V. Venkat Rao, V. Durga Kumari, S. Narayanan, Appl. Catal. 49 (1989) 165.
[12] F.C. Meunier, A. Yasmeen, J.R.H. Ross, Catal. Today 37 (1997) 33.
[13] J.C. Yori, J.M. Parera, Catal. Lett. 65 (2000) 205.
[14] K.T. Jung, A.T. Bell, Catal. Lett. 80 (2002) 63.
[15] K. Pokrovski, K.T. Jung, A/T. Bell, Langmuir 17 (2001) 4297.
[16] K.V.R. Chary, Ch. Praveen Kumar, D. Naresh, T. Bhaskar, Y. Sakata, J. Mol. Catal. A: Chem. 243 (2005) 149.
[17] K.V.R. Chary, G. Kishan, Ch. Praveen Kumar, G. Vidya Sagar, Appl. Catal. A: Gen. 246 (2003) 335.
[18] G.C. Bond, S.F. Tahir, Appl. Catal. A: Gen. 71 (1991) 1.
[19] J. Male, H.G. Niessen, A.T. Bell, T.D. Tilley, J. Catal. 194 (2000) 431.
[20] S.C. Su, A.T. Bell, J. Phys. Chem. B 102 (1998) 7000.
[21] K. Chen, S. Xie, E. Iglesia, A.T. Bell, J. Catal. 189 (2000) 421.
[22] B. Zhao, X. Xu, H. Ma, D. Sun, J. Gao, Catal. Lett. 45 (1997) 237.
[23] G. Centi, S. Perathoner, F. Trifiro, A. Aboukais, C.F. Aissi, M. Guelton, J. Phys. Chem. 96 (1992) 2617.
[24] M. Schraml-Marth, A. Wokaum, M. Pohl, H.L. Krauss, J. Chem. Soc. Faraday Trans. 87 (1991) 2635.
[25] M.M. Koranne, J.G. Goodwin Jr., G. Marcelin, J. Catal. 148 (1994) 369.
[26] H. Bosch, B.J. Kip, J.G. Van Ommen, P.J. Gellings, J. Chem. Soc. Faraday Trans. I 801 (1984) 2479.
[27] A. Baiker, P. Dollenmeir, M. Glinski, A. Reller, Appl. Catal. A: Gen. 35 (1987) 351.
[28] K.V.R. Chary, G. Kishan, T. Bhaskar, Ch. Sivaraj, J. Phys. Chem. 102 (1998) 6792.
[29] G.C. Bond, J.P. Zurita, S. Flamerz, P.J. Gellings, H. Bosch, J.G. Van Ommen, B.J. Kip, Appl. Catal. A: Gen. 22 (1986) 361.
[30] Y. Zhao, W. Li, M. Zhang, K. Tao, Catal. Commun. 3 (2002) 239.
[31] S. Velu, C.S. Swasmy, Appl. Catal. A: Gen. 145 (1996) 141.